ARMY RESEARCH LABORATORY

Visualization Techniques Applied to 155-mm Projectile Analysis

by Richard C Angelini and Sidra I Silton

ARL-TR-7137 November 2014

NOTICES

Disclaimers

The findings in this report are not to be construed as an official Department of the Army position unless so designated by other authorized documents.

Citation of manufacturer's or trade names does not constitute an official endorsement or approval of the use thereof.

Destroy this report when it is no longer needed. Do not return it to the originator.

Army Research Laboratory
Aberdeen Proving Ground, MD 21005-5067

ARL-TR-7137 **November 2014**

Visualization Techniques Applied to 155-mm Projectile Analysis

Richard C Angelini
Computational and Information Sciences Directorate, ARL

Sidra I Silton
Weapons and Materials Research Directorate, ARL

REPORT DOCUMENTATION PAGE	Form Approved OMB No. 0704-0188

1. REPORT DATE *(DD-MM-YYYY)*	2. REPORT TYPE	3. DATES COVERED (From - To)
November 2014	Final	October 2013–March 2014

4. TITLE AND SUBTITLE
Visualization Techniques Applied to 155-mm Projectile Analysis

5a. CONTRACT NUMBER

5b. GRANT NUMBER

5c. PROGRAM ELEMENT NUMBER

6. AUTHOR(S)
Richard C Angelini and Sidra I Silton

5d. PROJECT NUMBER
R.0006475.3

5e. TASK NUMBER

5f. WORK UNIT NUMBER

7. PERFORMING ORGANIZATION NAME(S) AND ADDRESS(ES)
US Army Research Laboratory
ATTN: RDRL-CIH-S
Aberdeen Proving Ground, MD 21005-5067

8. PERFORMING ORGANIZATION REPORT NUMBER
ARL-TR-7137

9. SPONSORING/MONITORING AGENCY NAME(S) AND ADDRESS(ES)

10. SPONSOR/MONITOR'S ACRONYM(S)

11. SPONSOR/MONITOR'S REPORT NUMBER(S)

12. DISTRIBUTION/AVAILABILITY STATEMENT
Approved for public release; distribution is unlimited.

13. SUPPLEMENTARY NOTES

14. ABSTRACT
Rolling projectiles using movable lifting surfaces for maneuver control have been and are continuing to be developed by the US Army. The aerodynamic characterization associated with the airframe development is more difficult than that of the traditional symmetrical, ballistic projectile because of the inherent asymmetries of the design as well as of the flow interactions. High fidelity computational simulations of the flow field around the projectile were completed in an attempt to begin to understand the variable nature of the aerodynamics associated with this rolling guided munition, particularly the intermittent dynamic instability suffered by the 155-mm precision munition. Visual analysis of these simulations is a critical component to understanding the complex phenomena demonstrated via these numerical calculations. The ability to understand the physics that impact the flight dynamics of the projectile through interactive manipulation of the computational model and more complex time-dependent analysis provides a more comprehensive understanding of the results. This report describes techniques for visualizing the unique characteristics of this complex guided munition.

15. SUBJECT TERMS
projectile analysis, scientific visualization, ensight

16. SECURITY CLASSIFICATION OF:			17. LIMITATION OF ABSTRACT	18. NUMBER OF PAGES	19a. NAME OF RESPONSIBLE PERSON
a. REPORT	b. ABSTRACT	c. THIS PAGE			Richard C Angelini
Unclassified	Unclassified	Unclassified	UU	30	19b. TELEPHONE NUMBER (*Include area code*) 410-278-6266

Standard Form 298 (Rev. 8/98)
Prescribed by ANSI Std. Z39.18

Contents

List of Figures

List of Tables

Acknowledgments

This work was supported in part by a grant of high-performance computing time from the US Department of Defense (DOD) High-Performance Computing Modernization program at the US Army Research Laboratory (ARL) DOD Supercomputing Resource Center (DSRC), Aberdeen Proving Ground, MD, and the US Air Force Research Laboratory (AFRL) DSRC, Wright Patterson Air Force Base, Dayton, OH.

INTENTIONALLY LEFT BLANK.

1. Introduction

Precision munition research is currently an area of focus throughout the United States armed services. Within the US Army, rolling projectiles using movable lifting surfaces for maneuver control are continuing to be developed.[1, 2] The aerodynamic characterization associated with the airframe development is more difficult than that of the traditional symmetrical, ballistic projectile because of the inherent asymmetries of the design and the flow interactions caused by the projectile. A thorough understanding of the flight behavior of such a projectile is necessary to ensure that it can be guided to the desired point in space. This understanding can often prove to be a challenge.

While analyzing data collected during the flight of 1 such rolling airframe with aerodynamic asymmetry, the nonlinear dynamic side moment was found to be extremely sensitive to minor differences in angle of attack, especially in the transonic flight regime. This sensitivity manifested itself as a large round-to-round variation in flight behavior; some rounds exhibited near constant magnitude yawing motion, while others exhibited significant increases. In addition to the standard counter-clockwise coning motion exhibited, there was even a reversal of coning direction that was detected mid flight on a few rounds in the subsonic flight regime. The analysis of the flight experiments was unable to determine the flow mechanisms responsible for the coning reversal, although it was attributed to an unverifiable static side moment.

In an attempt to begin to understand the variable nature of the aerodynamics associated with this rolling guided munition, particularly the intermittent dynamic instability suffered by the 155-mm precision munition (Fig. 1), high-fidelity numerical simulations of the flow field around the projectile were completed. In addition to obtaining the static and dynamic ballistic coefficients, significant effort was spent on analyzing the flow field around the projectile. This report focuses on the efforts spent to develop the necessary techniques to visualize the flow of particles as they leave the trailing edge of the canard and are swept downstream over the fins during the transient rolling simulations at angle of attack.

Fig. 1 The 155-mm experimental projectile from flight Test 2

2. Geometry and Computational Methodology

2.1 Projectile Configurations and Test Conditions

A simplified version of the 155-mm Very Affordable Precision Projectile (VAPP) experimental projectile was created in SolidWorks[3] for use in the computational fluid dynamics (CFD) study presented herein (Fig. 2). All screw holes were removed from the projectile model, the canards were attached flush to the body, the fins were attached flush to the hub (no hinges), and all interior components were removed. However, the projectile reference properties remained the same as those of the experiment and are included here for reference in the Table below.

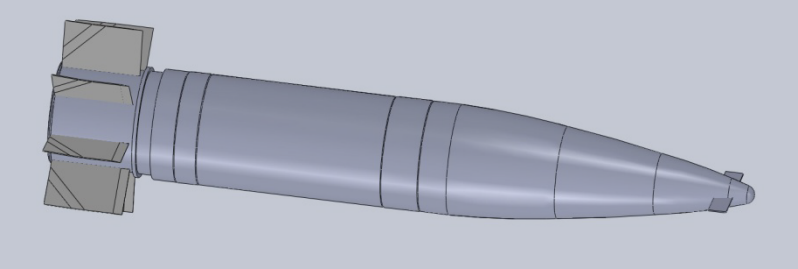

Fig. 2 Simplified CFD model for 155-mm experimental projectile

Table Projectile reference properties

Projectile Physical Properties	**Value**
Diameter, d (m)	0.155
Length, L (mm)	0.9814
Mass, m (kg)	44.197
Center of gravity, X_{cg}	0.5976
Axial moment of inertia, I_{xx} (kg-m^2)	0.1664
Transverse moment of inertia, I_{yy} (kg-m^2)	2.2712

The removal of the interior components is possible as they do not affect the aerodynamics of the projectile. There are times, however, when presenting results to managers or potential customers that it is desirable not only to see the external aerodynamic shape but also to see the internal control actuation system (CAS) (Fig. 3). The CAS is the portion of the projectile that is designed to allow motion of the movable lifting surfaces. Visualizing both the internal structure and the external aerodynamic flow field allows the integrated and complicated nature of a precision munition to be better understood.

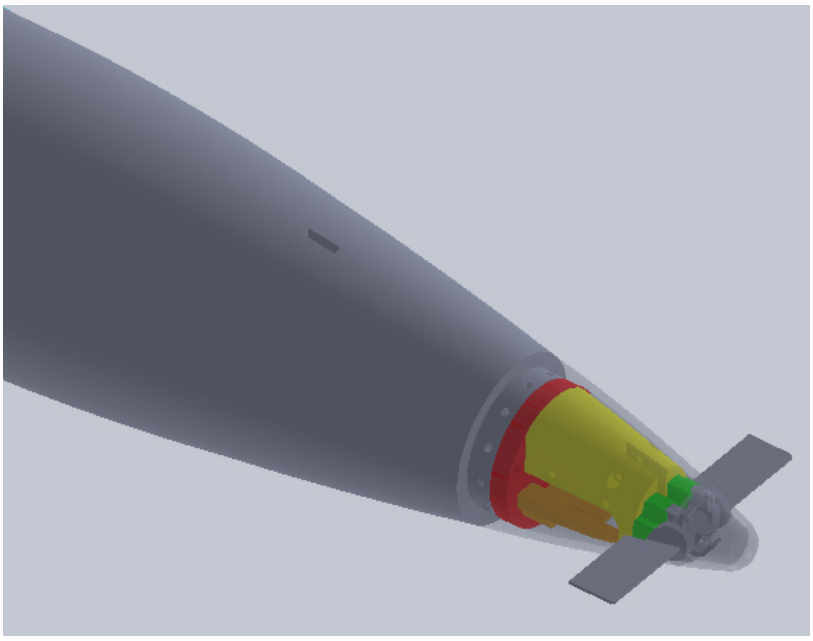

Fig. 3 Forward portion of solid model representation of 155-mm experimental projectile showing CAS

The visualizations presented in this report are for Mach 0.98 at 5° angle of attack, although additional angles and Mach number were investigated. Those investigations will be presented in detail as part of a later report. The free stream static pressure, P, and temperature, T, were set to 101325 Pa and 288.15 K, respectively.

2.2 Computational Domains and Boundary Conditions

An unstructured computational domain (i.e., mesh) was created for the geometry described above using the MIME[4] mesh generator from Metacomp Technologies. The domain utilized the outer boundary shown in Fig. 4 and the surface mesh spacing and density boxes shown in Fig. 5. This mesh, which contained 64.2 million cells, specified the first cell spacing to be 0.75 μm, which ensured the y^+ was less than 1 everywhere.

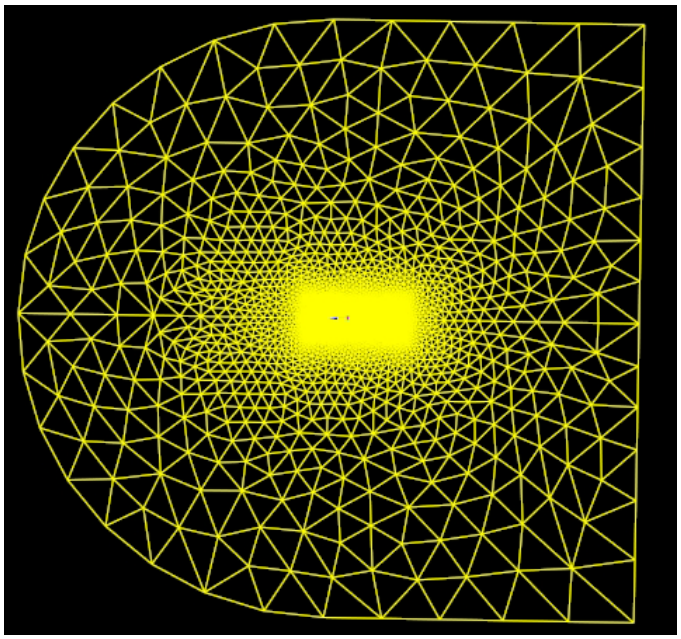

Fig. 4 Unstructured MIME mesh used for simulations

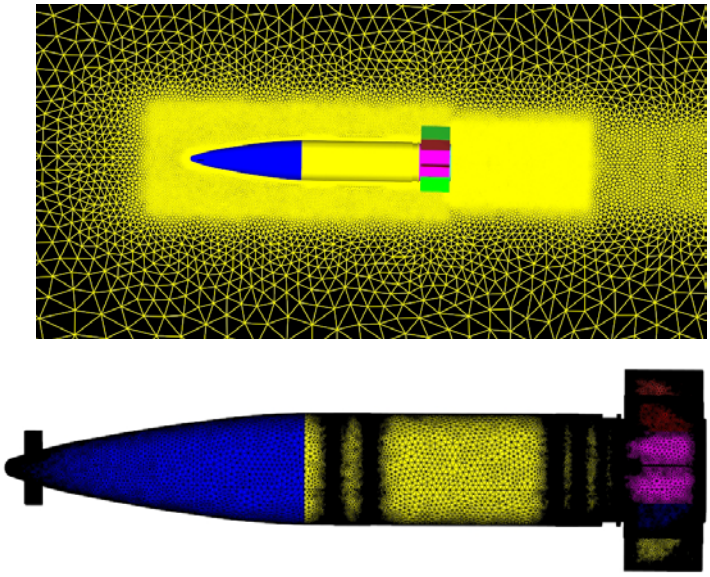

Fig. 5 Close up of projectile for unstructured mesh showing locations of density boxes (top) and surface mesh (bottom)

The mesh was discretized to facilitate parallel computations on 400 processors. The computations were performed on HAROLD, a SGI Altix ICE 8200 supercomputer composed of 2.8-GHz Intel Xeon Nehalem processors, and RAPTOR, a Cray XE6 supercomputer composed of 2.5-GHz AMD Opteron processors. HAROLD is housed and managed by the US Army Research Laboratory's (ARL's) Department of Defense (DOD) Supercomputing Resource

Center (DSRC), Aberdeen Proving Ground, MD. Raptor is housed and managed by the US Air Force Research Laboratory's (AFRL's) DSRC at Wright Patterson Air Force Base, Dayton, OH.

The wall boundary conditions of the projectiles were set as a stationary no-slip, adiabatic condition relative to the mesh motion. Additionally, the walls were specified as solve-to-the-wall. The farfield boundaries were each specified using Metacomp Technologies'[5] characteristics-based inflow/outflow boundary condition, which is based on solving a Riemann problem at the boundary.

2.3 Numerics

Rolling/spinning is the motion whereby the projectile flies at a constant angle, α, with respect to the freestream vector while undergoing a constant angular rotation, $\dot{\phi}$, about its body-fixed *x*-axis. Therefore, the angular rotation is equal to the spin rate, *p*. It is this spin component that produces the roll-induced side moment.[6,7] An accurate understanding of the flow physics that produces the roll-induced side moment is a critical component in the development of precision munitions. It is possible to replicate the spin component of the projectile in simulations using time-dependent spinning motion.

The simulations were completed using the commercially available code, CFD^{++} v11.1.1[5], from Metacomp Technologies. The CFD^{++} code can simulate a range of fluid dynamic phenomena, ranging from incompressible to hypersonic flow. The 3-D, time-dependent RANS equations are solved using the finite volume method.[8] The spatial discretization was a second-order, multidimensional total variation diminishing (TVD) polynomial interpolation scheme. Solutions to semi-infinite Riemann problems are used in CFD^{++} to provide upwind flux information to the underlying transport scheme. Approximate Riemann solvers are used to determine the higher order fluxes to avoid spurious oscillations that may become physically unbounded if determined via fixed-stencil interpolation. The 2-equation realizable k-ε model, which solves the transport equations for k (turbulent kinetic energy) and ε (dissipation rate), was chosen as the turbulence closure model. Steady-state simulations using the double precision, point-implicit scheme were completed during the course of the computational study. The steady-state solution was used as the starting solution for the time-dependant simulations.

The time-dependant, rolling simulation required the roll rate, *p*, and timestep, Δt, as inputs. The roll rate was specified on the order of p_{eq}, which was determined to be 18.3 Hz (114.982 rad/s). The number of global iterations per rotation, N, was chosen based on characteristic time, which took into consideration both the projectile length and rotation rate (Strouhal number was not considered at this time as the wake flow was not considered to be overly important). As such, 720 global iterations were chosen for the Mach 0.98 simulations presented here. Using 720 global iterations per rotation limited the rotation to 0.5° per timestep, while still allowing 35 timesteps for the flow to traverse the length of the body. The timestep, $\Delta t = 7.590 \times 10^{-5}$sec, used in the simulations is calculated from Eq. 1. For this time accurate simulation, 20 inner

iterations were necessary to obtain 0.5–1 order of magnitude reduction in the cell-averaged inner residuals of the RANS equations.

$$\Delta t = \frac{T}{N} = \frac{\pi d}{NVk}. \quad (1)$$

To ensure a converged solution, simulations were completed for 2 rotation cycles (720° or 4π). The results flow was analyzed over the last cycle. For the final analysis, a full solution output file was generated at each timestep. Having the flow field solution output at each timestep ensured that the flow could be tracked along the body to investigate the interaction of the flow being shed from the canards as it impacted the fins, as it only took 35 timesteps for the flow to move over the entire length of the projectile.

3. Methodology for Pathlines

Visual analysis of these simulations is a critical component to understanding the complex phenomena demonstrated through these numerical calculations. The ability to understand the physics that impact the flight dynamics of the projectile through interactive manipulation of the computational model and more complex time-dependent analysis provides a more comprehensive understanding of the results. The visualization software package, EnSight, from Computational Engineering International (CEI), has been in use at the ARL since the early 1990s. EnSight has been a valuable tool for postprocessing computational simulations generated on high-performance computing systems. It is particularly adept at processing results generated to support CFD simulations.[9] EnSight supports traditional visual analysis techniques, such as isosurface generation, clip planes, and particle traces, which are essential for visualizing results generated for this 155-mm projectile analysis.

Particle trace animations are often used to demonstrate air flow around a flying object. A particle trace represents the path a massless particle would take if released in a flow field. From an initial seed point (the emitter), a path is formed by integrating through the velocity field over time. The path is therefore everywhere parallel to the flow. Traces calculated in a steady-state flow field are called streamlines. For transient flow, the path is known as a pathline. (CEI OnLine Help Manual). Particle seed points can be from a single point in space, or equally spaced along a line or clip plane defined within the computation mesh. Seed points can also be defined based on the parts defined within the computational mesh. For instance, it is possible to randomly generate particle seed points from a part that represents a canard on the front of a projectile, or from a fin at the rear of a projectile. EnSight provides numerous methods for defining how these particle seed points can be defined.

For this particular analysis, it was determined that particle traces should be emitted from the canard parts in the computational mesh and that the results would be viewed as pathlines

following the resulting particles through the transient dataset. This task was complicated by the fact that the projectile was spinning so that each timestep changed the location of the emitter seed points to a different location in the mesh. EnSight was able to accommodate the dynamic location of the emitter seed points through a multistep process.

- Identify emitter parts.
- Create an external file that represented the emitters seed point locations for each timestep.
- Calculate pathlines based on external emitter file.
- Customize pathlines to represent particle animation paths.
- Save particle animation over time.

Identifying the emitter parts and how those seed points are to be emitted can also be very challenging and computationally expensive. The most direct and easiest approach is to identify the computational part or parts (i.e., the canards) and allow EnSight to randomly select seed points. Figure 6 shows steady state streamlines using randomly generated seed parts from the canards. To generate seed points across the transient dataset, EnSight command language is used to generate an external emitter file.

- Use EnSight graphical user interface (GUI) to select those parts to be used as a source of the emitter seed points.
- Use EnSight command language to generate the external emitters file from the GUI.

  File-> Command

- Follow the general form of the EnSight command.

  test: `build_emitters start-time end-time time-increment number-of-emitters` filename

In the specific example, below, EnSight has been tasked to generate 100 random seed points from the part(s) selected for 51 timesteps between time 0 and 50 and to save those seed points in the file `emitters.file`. The file `emitters.file` will be used later to actually generate the pathlines. The resulting emitter file contains the coordinate values for each emitter seeds point at each timestep in the simulation. These values are used by the internal EnSight pathline algorithms to calculate the position of each particle for each timestep in the transient dataset.

test: `build_emitters 0 50 1 100` emitters.file

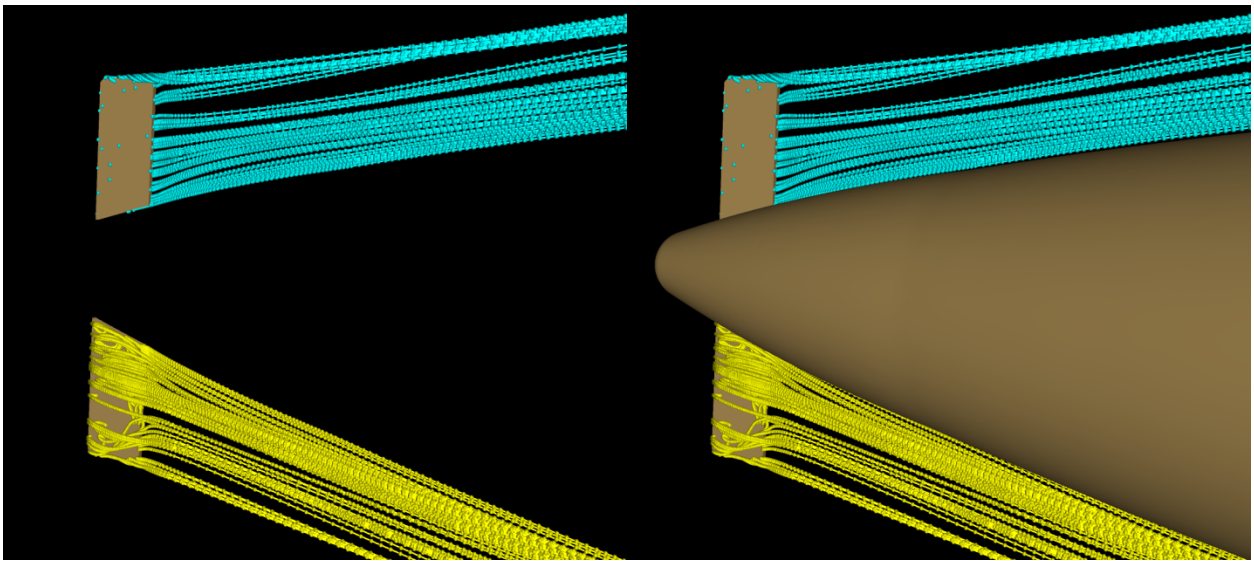

Fig. 6 Streamlines (particle traces at a single timestep) created using random seed points generated from the canard parts

An alternative solution for creating emitter seed points is to create an EnSight subset part of specifically chosen nodes from the mesh. For instance, if the region of interest is the trailing edge of the canard, specific nodes can be selected using the EnSight GUI. Those nodes are also used to create a subset part (Fig. 7). The pathlines/streamlines are then generated using that subset part as the emitter seed values (Fig. 8).

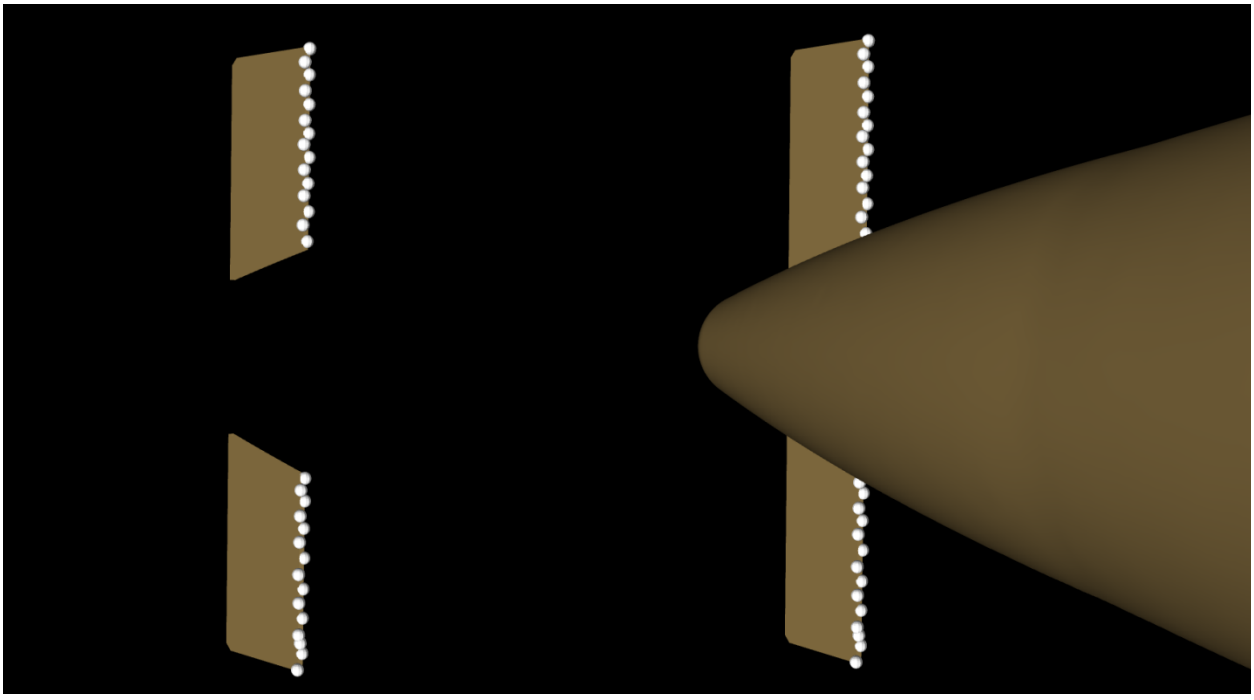

Fig. 7 Emitter seeds selected along trailing edge of canard used to generate a subset part to create pathlines. Image on the left shows the canards; image on the right, the canards and projectile body.

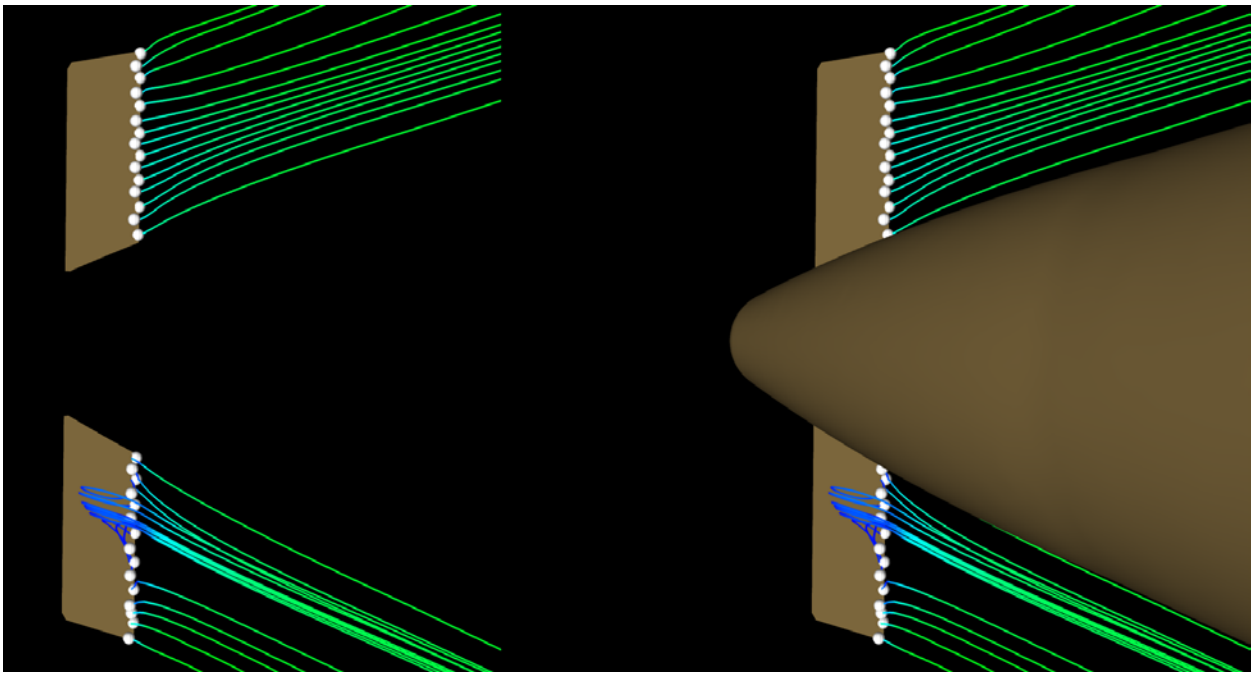

Fig. 8 Streamlines created using subset parts as the emitter seed origin

The result of either of these methods is a series of pathlines generated from the emitter seed locations across the entire time domain of the transient dataset. In Fig. 9, the pathlines are visible for each timestep as the projectile rotates and the particles are emitted from the trailing edge of the canard at each timestep. The final step in the process is to animate the results—the pathlines are turned off and replaced with sphere or arrow glyphs; those glyphs are integrated over time based on the calculation of the pathlines. Fig. 10 represents a single frame of a pathline animation, showing the sphere glyphs following the integrated pathlines.

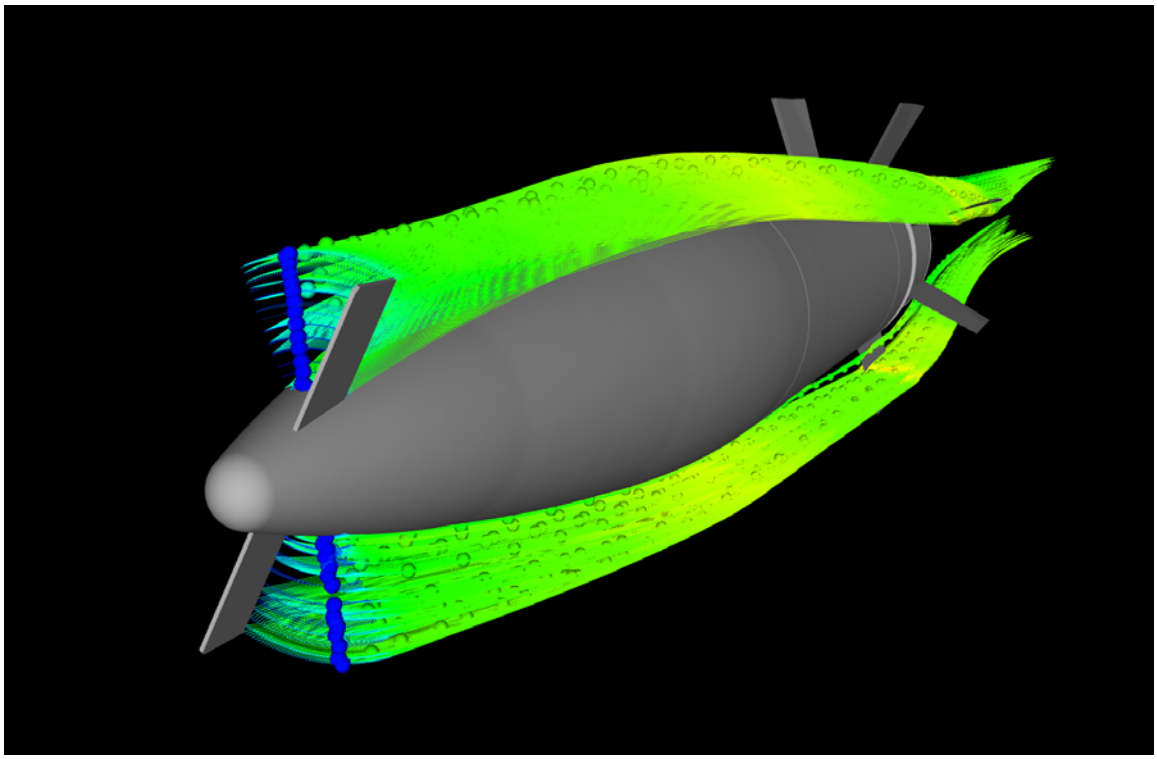

Fig. 9 Visible pathlines for each timestep as they are emitted from the trailing edge of the canards

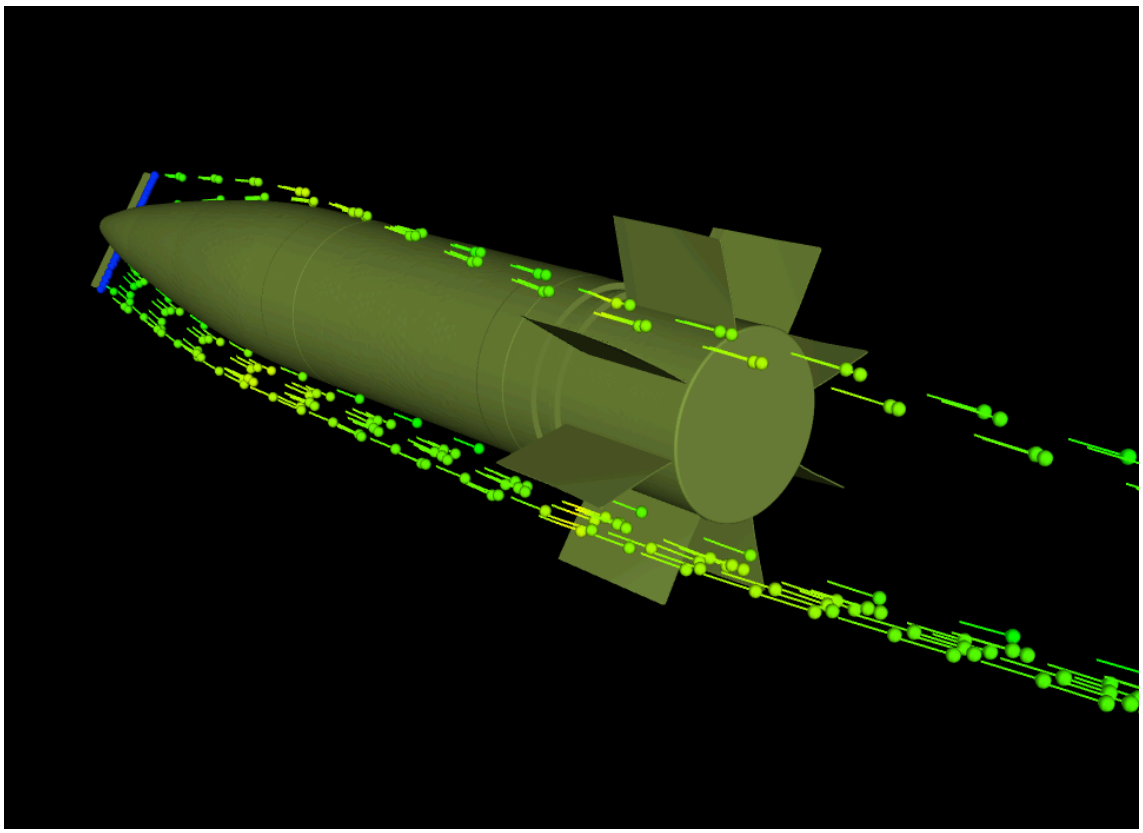

Fig. 10 A single frame from the pathline animation

4. Methodology for Computer-Aided Design (CAD) Geometry Overlay

As described earlier, the computational mesh was simplified by removing the internal components so that visualizing those internal components in conjunction with the external aerodynamic flow field allowed the integrated and complicated nature of a precision munition to be better understood. Because these internal components are typically not available during the traditional visualization analysis process, they are often overlooked. The ability to combine the computational results with the complex CAD model allows for a more complete understanding of the problem being analyzed.

EnSight has the ability to read in certain common CAD data formats (.OBJ, .STL); however, the ability to align portions of the computational mesh with CAD geometry was not supported. The requirement to replace the basic computational mesh with the more complex CAD geometry presented a challenge. The problem was described to CEI application specialists and they were able to develop a method to align the CAD geometry with the computational mesh based on identifying 3 nodes common to the mesh and the CAD geometry. EnSight developers were able to provide guidance on how to choose those 3 nodes in such a way as to provide a very close alignment of the CAD model over the computational mesh.

EnSight also has the ability to read multiple datasets into a single analysis session using the concept of cases. Each case is responsible for reading a particular dataset; those datasets do not need to reside on the same system. In this case, the original computation results were residing on a common shared file system that is accessible by all of the high performance computing systems. As such, that data was read using EnSight server-of-servers (SOS) from the ARL Utility Server. The CAD geometry resided on the local workstation file system; a single local EnSight server was used to read in those results.

Once both datasets were read into EnSight, the methodology required that corresponding nodes from the same components in the projectile configuration and the CAD geometry be identified. Using 1 of the projectile canards, 3 corresponding nodes were identified; using those nodes, the CAD geometry was able to be aligned with the computational mesh using EnSight command language. The command dialog in the graphical user interface was used to enter the command is

test: align parts 23 14 12 11 20 98 97 99.

The syntax of this command identifies the part number and the 3-+ node values that are to be used to align the parts. In this example, Parts 23 and 20 represent the 2 corresponding geometric entities to be used to align the computational mesh with the CAD geometry. Part 23, nodes 14, 12, and 11, are aligned with Part 20, nodes 98, 97, and 99 (Fig. 11).

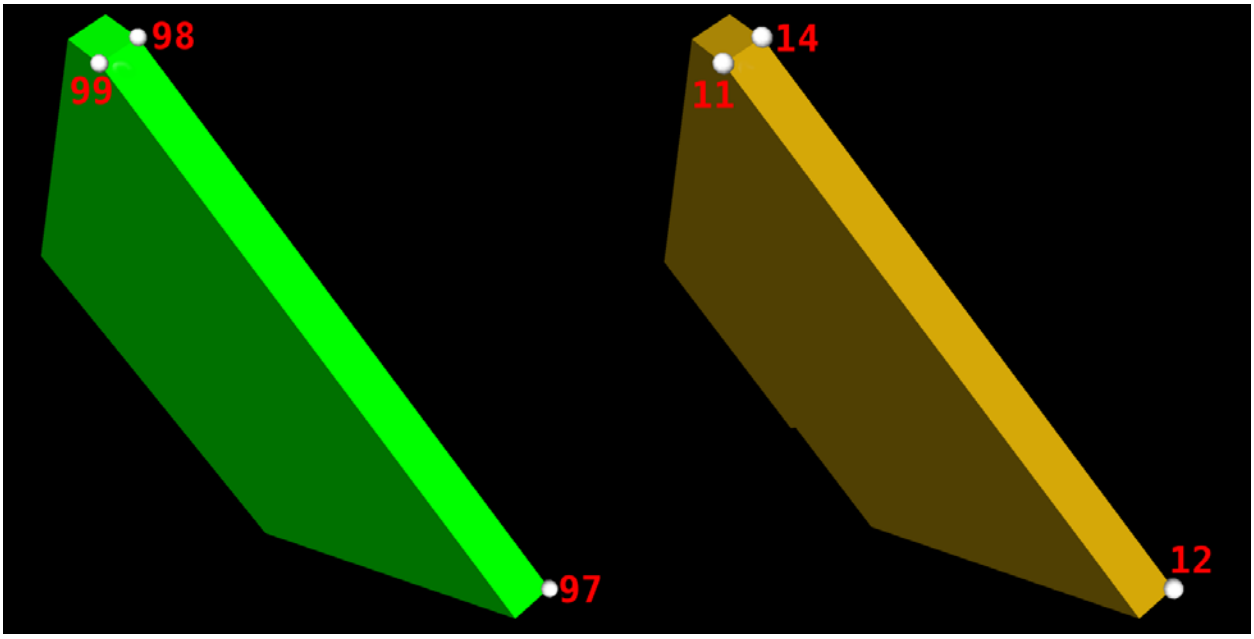

Fig. 11 Part 20 (original computational mesh), left, with nodes clockwise 98, 97, and 99 highlighted; part 23 (CAD model), right, with nodes clockwise 14, 12, and 11 highlighted. These nodes are used to align the CAD geometry with the computational mesh.

The final results of aligning the CAD geometry with the corresponding computational parts can be seen in Fig. 12. The CAD geometry aligns properly with the computational parts and will maintain the proper alignment on a transient dataset. As the projectile rotates, pitches, and/or yaws over time, the CAD geometry will maintain proper alignment because of nodal alignment established by the EnSight command language.

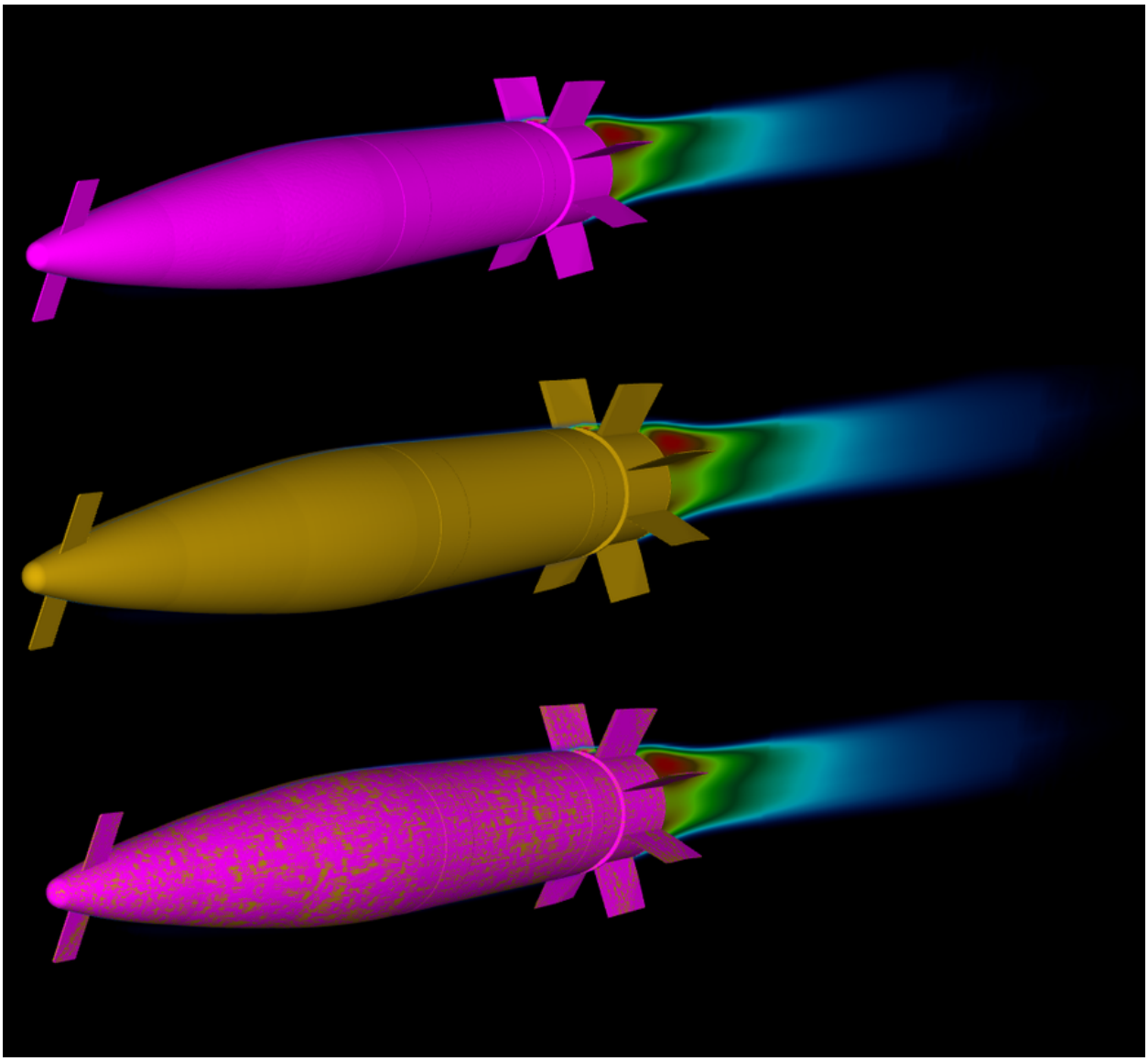

Fig. 12 Final projectile alignment. The top image shows the orientation of the projectile within the original computational mesh. The middle image shows the alignment of the CAD geometry in the proper position. The bottom image shows both the projectile and the CAD geometry and verifies that the alignment is correct.

5. Conclusions

Simulations were completed that demonstrate the variable nature of the aerodynamics associated with this rolling guided munition, with particular focus on the intermittent dynamic instability suffered by the 155-mm precision munition. In addition to obtaining the static and dynamic ballistic coefficients, analysis of the flow around the projectile also occurred. Significant effort was expended in developing the methodologies necessary to visualize the complex flow around

this munition. Developing pathline animations of particles emitted from rotating canards was a very difficult task—a computational exhaustive, multistep process (see the appendix for the video of the animation). Identifying emitter locations for the pathline seeds on a moving munition required customized software from the developers of EnSight. That functionality was rolled into subsequent releases of the production software. The second part of this analysis process was to provide a methodology for overlaying more complex CAD geometry over the simpler surface geometry of the munition used in the computation. Visualizing both the internal structure and the external aerodynamic flow field allows the integrated and complicated nature of a precision munition to be better understood as part of the visual analysis process.

6. References

1. Fresconi F, Brown T, Celmins I, DeSpirito J, Ilg M, Maley J, Magnotti P, Scanlan, A, Stout C, Vazquez E. Very affordable precision projectile system and flight experiments. Proceedings of the 27th Army Science Conference; Orlando, FL, 2010.
2. Fresconi F, Harkins T. Experimental flight characterization of asymmetric and maneuvering projectiles from elevated gun firings. Journal of Spacecraft and Rockets. 49(6):1120–1130.
3. Dassault Systèmes SOLIDWORKS Corp. SolidWorks User Manual, Waltham, MA, 2010.
4. Metacomp Technologies, Inc. MIME User Manual, Agoura Hills, CA, 2010.
5. Metacomp Technologies, Inc. "CFD^{++} User Manual, Agoura Hills, CA, 2011.
6. Platou AS. Magnus characteristics of finned and nonfinned projectiles. AIAA Journal. 1965; 3(1):83–90.
7. Pechier M, Guillen P, Cayzac R, Magnus effect over finned projectiles. J. of Spacecraft and Rockets. 2001;38(4):542–549.
8. Peroomian O, Chakravarthy S, Palaniswamy S, Goldberg U. Convergence acceleration for unified-grid formulation using preconditioned implicit relaxation. AIAA Paper 1998-0116. Proceedings of the 36th Aerospace Sciences Meeting and Exhibit. 1998 Jan 12-14; Reno, NV.
9. Angelini RC, Sahu J. Visualization techniques of a CFD++ data set of a spinning smart munition. Aberdeen Proving Ground (MD): Army Research Laboratory (US); December 2004. Report No.: ARL-TR-3380. Also available at http://www.arl.army.mil/www/default.cfm?technical_report=356.

INTENTIONALLY LEFT BLANK.

Appendix. Animation of Results

Animations were created from the solution files generated by the computational fluid dynamics (CFD) solver for the time-accurate rolling simulations at each timestep for the Mach 0.98, $\alpha = 5°$ configuration. The final animations overlaid velocity pathlines initiated from the canards and Mach volumes. The Mach volumes allow visualization of the shock waves that are present in a transonic flow field and show how the shock waves affect the particle paths generated from the canards. The particle paths emitted from the canards move down stream with time and are affected by the shock waves as well as by the rolling motion of the projectile. The particle paths cross over the fins causing the interaction effects of the canards on the fins. Understanding these interaction effects is critical to the understanding of the projectile aerodynamics.

The use of 3 viewpoints in the animation allows for simultaneous viewing of the important phenomena that are occurring. The main animation shows the entire projectile. The air is flowing over the projectile from right to left and the rolling motion of the projectile is clockwise looking from the aft end of the projectile towards the nose. The pathlines move over the body and are affected by both the air flow moving over the projectile as well as by the rolling motion of the projectile. As the pathlines reach the aft end of the body, the direction of flow is turned, but the pathlines remain clear of the wake (i.e., the air flow over the body is not sucked into the wake). While the main animation provides an overview as to what is happening, detail is lacking. Thus, close-ups are provided.

In the top left video, the particles are coming towards the reader and the projectile is rotating clockwise. It is easy to see that there is initially no interaction between the particles emitted from the canards. As the projectile rotates, the pathlines are pulled across the fins, which cause the interaction effects between the canards and the fins. Additionally, the pathlines are bent as they pass through the fins but the reason they bend is unclear.

In the top right video, the reader is looking from the nose towards the fins, which is why the fins appear to be turning counter-clockwise. The cause of the bend as the pathlines pass the fins is obvious in this view. The pathlines are passing through the shock waves that are generated by the fins. In fact, the shock waves that sit in front of the fins and radiate away from each of the fins interact with each other causing shock-shock interactions. The shock-shock interactions, of course, would not occur in purely subsonic flow. However, they obviously play a significant role in transonic and supersonic flow and affect the canard-fin interaction as well.

Click on the image to start the video.

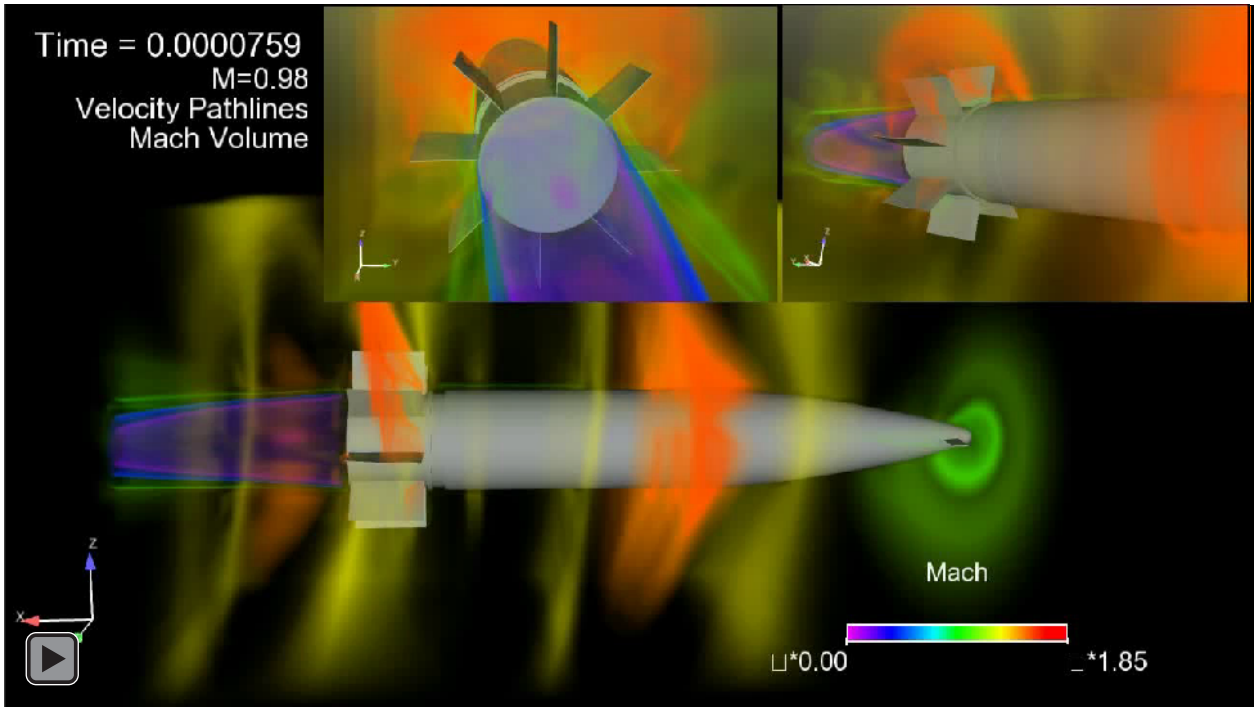

INTENTIONALLY LEFT BLANK.

List of Symbols, Abbreviations, and Acronyms

AFRL	US Air Force Research Laboratory
ARL	US Army Research Laboratory
CAD	Computer-Aided Design
CAS	control actuation system
CEI	Computational Engineering International
CFD	computational fluid dynamics
DOD	Department of Defense
DSRC	DOD Supercomputing Resource Center
GUI	graphical user interface
SOS	server-of-servers
TVD	total variation diminishing
VAPP	Very Affordable Precision Projectile
Δt	timestep (s)
P	pressure (Pa)
p	roll rate (rad/s)
p_{eq}	equilibrium roll rate (rad/s)
N	number of global iterations per rotation
T	temperature (K)
d	diameter (m)
V	velocity (m/s)
α	angle of attack (degree)
$\dot{\phi}$	angular rotation (degree/s)

1 (PDF)	DEFENSE TECHNICAL INFORMATION CTR DTIC OCA
2 (PDF)	DIRECTOR US ARMY RESEARCH LAB RDRL CIO LL IMAL HRA MAIL & RECORDS MGMT
1 (PDF)	GOVT PRINTG OFC A MALHOTRA
10 (PDF)	DIR USARL RDRL CIH S R ANGELINI D SHIRES L BRAINARD RDRL WML E S SILTON F FRESCONI J DESPIRITO V BHAGWANDIN P WEINACHT J SAHU B GUIDOS